Available online at www.sciencedirect.com

ScienceDirect

IFAC Papers Online CONFERENCE PAPER ARCHIVE

IFAC-PapersOnLine 49-8 (2016) 290–297

Piezoelectric beam with distributed control ports: a power-preserving discretization using weak formulation. ⋆

Flávio Luiz Cardoso-Ribeiro *,⋆⋆ **Denis Matignon** * **Valérie Pommier-Budinger** *

* *Institut Supérieur de l'Aéronautique et de l'Espace (ISAE-Supaero), Université de Toulouse, 31055 Toulouse Cedex 4, France (e-mail: flaviocr@ita.br, Denis.Matignon@isae.fr, Valerie.Budinger@isae.fr)*

Abstract: A model reduction method for infinite-dimensional port-Hamiltonian systems with distributed ports is presented. The method is applied to the Euler-Bernoulli equation with piezoelectric patches. The voltage is considered as an external input of the system. This gives rise to an unbounded input operator. A weak formulation is used to overcome this difficulty. It also allows defining a discretization method which leads to a finite-dimensional port-Hamiltonian system; the energy flow of the original system is preserved. Numerical results are compared to experimental ones to validate the method. Further work should use this model to couple the approximated equations with a more complex system, and to design active control laws.

Keywords: Model Reduction for Control, Port-Hamiltonian systems, Piezoelectric materials.

1. INTRODUCTION

This paper is part of ongoing research in modeling and control of fluid-structure interactions. This topic is a major concern in several engineering applications. The coupling of aerodynamics and structural dynamics, for example, can lead to instability and structural loss in systems as diverse as airplanes and suspension bridges.

At ISAE, we have an experimental device that consists of an aluminum plate with a water tank near its free-tip. The fluid dynamics and structural dynamics have similar natural vibration frequencies, leading to strong coupling between them. Piezoelectric patches are attached to the plate to perform active control.

In a previous work (see Cardoso-Ribeiro et al. (2015)), we have modeled the fluid-structure system using the port-Hamiltonian systems (pHs) formulation. The motivation for using this formulation was that it allows describing each element of the system separately and to connect them easily. Each subsystem is described using pHs formulation. Physically relevant variables appear as interconnection ports and the different subsystems are coupled, guaranteeing that the global system is also a pHs. Finally, pHs provide a natural framework for using energy-based methods for control purposes (see e.g. Duindam et al. (2009)).

The piezoelectric actuators were not modeled in our previous work. The main goal of this paper is to find a finite-dimensional piezoelectric model that preserves the port-Hamiltonian structure of the infinite-dimensional system.

Modeling of beams with piezoelectric patches is well known in the literature (see for e.g. the papers of Aglietti et al. (1997), and Preumont (2011)).

Several previous contributions were presented in the last years for modeling and discretization of a beam with piezoelectric patches as a pHs (see e.g. Macchelli et al. (2004), Voss and Scherpen (2011), Voss and Scherpen (2014), Morris and Ozer (2013)).

In this contribution, voltage is used as an external control input of the piezoelectric material. This comes with a difficulty, since an unbounded input operator appears. This problem was avoided in the previous articles using two different strategies: 1) by including the electric field (which is equivalent to the voltage) as a dynamic variable, instead of an input; 2) by including the magnetic field dynamics. The first solution allows the simulation, but leads to a finite-dimensional approximation that is not stabilizable (see Voss and Scherpen (2011) and Voss (2010)). The second solution introduces dynamic states of high frequency (that usually does not affect the dynamics in the frequency range of interest in mechanical problems). After spatial discretization, both solutions lead to constrained state-space systems, in the form of Differential Algebraic Equations (DAE), since the piezoelectric voltage is an output of these systems.

This work uses only the mechanical variables as energy variables. The final finite-dimensional system has voltage as an input. The finite-dimensional state-space obtained does not have any constraints related to the voltage.

The spatial discretization presented here is based on the work of Moulla et al. (2012). They used modified

⋆ The contribution of the authors has been done within the context of the French National Research Agency sponsored project HAMECMOPSYS. Further information is available at http://www.hamecmopsys.ens2m.fr/.

**Flávio is on a leave from Instituto Tecnológico de Aeronáutica, with financial support from CNPq-Brazil.

2405-8963 © 2016, IFAC (International Federation of Automatic Control) Hosting by Elsevier Ltd. All rights reserved.
Peer review under responsibility of International Federation of Automatic Control.
10.1016/j.ifacol.2016.07.456

classical pseudo-spectral methods (see e.g. Boyd (2001) and Trefethen (2000)) to preserve the port-Hamiltonian structure of the infinite-dimensional pHs at the discrete level. The method is extended here in a number of ways:

(1) the work of Moulla et al. (2012) deals only with first-order derivative operators. Here, second-order operators are used;
(2) the discretization of distributed ports is included;
(3) a weak formulation is used to overcome the issue linked to the differential operator that is applied to the nonsmooth input ports.

We show that the resulting finite-dimensional approximated system preserves the port-Hamiltonian structure of the original system.

To validate our approach, the numerical method is implemented and compared to experimental results.

2. PIEZOELECTRIC BEAM EQUATIONS

This section is divided in three parts. Firstly, the partial differential equations for the piezoelectric beam are obtained from Hamilton principle. Secondly, the equations are written using the port-Hamiltonian formalism, and it is shown that the energy flows through the boundary and distributed ports. Finally, the equations are rewritten using a weak formulation in § 2.3.

2.1 Derivation of equations from Hamilton Principle

Let us consider a beam with a piezoelectric patch attached to its surface, as presented in Fig. 1.

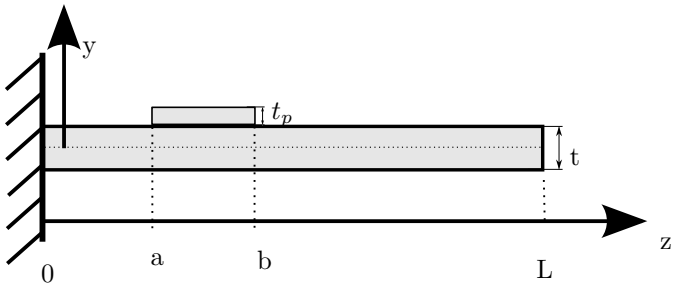

Fig. 1. Beam with piezoelectric patch.

The beam has the following properties: length L, thickness t, width b, section area $S = bt$, density ρ. The patch has the following properties: length $b - a$, thickness t_p, width b_p, section area $S_p = b_p t_p$, density ρ_p.

The beam vertical deflection is given by $w(z,t)$. Neglecting the rotational inertia, the kinetic energy is given by:

$$\begin{aligned}\mathcal{K} &= \frac{1}{2}\int_\Omega \rho \dot{w}^2 \,\mathrm{d}V\,,\\ &= \frac{1}{2}\int_{z=0}^{L} \left(\rho S + \rho_p S_p \Pi_{ab}(z)\right)\dot{w}^2 \,\mathrm{d}z\,,\end{aligned} \tag{1}$$

where $\dot{w}$ is the time-derivative of $w(z,t)$ and $\Pi(z)$ is the rectangular function, defined as:

$$\Pi(z) := \begin{cases} 0, & z \le a \\ 1, & a < z < b \\ 0, & b \le z \end{cases} \tag{2}$$

It is assumed that the strain ϵ is only due to bending, such that: $\epsilon = -y\,\partial^2_{z^2} w(z,t)$. In this case, the potential elastic energy is:

$$\mathcal{P} = \frac{1}{2}\int_\Omega \sigma_{mec}\epsilon \,\mathrm{d}V\,, \tag{3}$$

where $\sigma_{mec} = E_i\,\epsilon$ is the mechanical stress (E_i is the material elasticity modulus). After integration over the cross-sectional area:

$$\mathcal{P} = \frac{1}{2}\int_{z=0}^{L} \left(EI + \Pi_{ab}(z) E_p I_p\right)\left(\partial^2_{z^2} w\right)^2 \mathrm{d}z\,, \tag{4}$$

where E and E_p are the elasticity modulus of the beam and the piezoelectric patch, I and I_p are the area moments of inertia, with respect to the neutral axis ($y = 0$):

$$\begin{aligned} I &= b\int_{y=-t/2}^{t/2} y^2 \,\mathrm{d}y = \frac{bt^3}{12}\,,\\ I_p &= b_p\int_{y=t/2}^{t/2+t_p} y^2 \,\mathrm{d}y = b_p\left(\frac{(t/2+t_p)^3}{3} - \frac{t^3}{24}\right)\end{aligned} \tag{5}$$

The work due to the voltage $v(z,t)$ applied to the piezoelectric patch is given by:

$$\mathcal{W} = \frac{1}{2}\int_\Omega \sigma_{elec}\epsilon \,\mathrm{d}V\,, \tag{6}$$

where $\sigma_{elec} = -\gamma E_y(z,t)$ ($E_y(z,t)$ is the electric field in the y direction, γ is the piezoelectric electro-mechanical constant). It is assumed that the electric field is proportional to the voltage applied to the piezoelectric patches: $E_y(z,t) = \frac{v(z,t)}{t_p}$. This leads to the following work expression:

$$\mathcal{W} = \frac{1}{2}\int_{z=0}^{L} \gamma\frac{v(z,t)}{t_p}\Pi_{ab}(z) I_{p,1}\,\partial^2_{z^2} w \,\mathrm{d}z\,, \tag{7}$$

where $I_{p,1}$ is the first moment of area of the piezoelectric patch, i.e.,

$$I_{p,1} = b_p\int_{y=t/2}^{t/2+t_p} y\,\mathrm{d}y = \frac{b_p t_p}{2}(t + t_p)\,. \tag{8}$$

The Hamilton Principle (see e.g. Geradin and Rixen (2015)), i.e.,

$$\delta\int_{t_1}^{t_f} (\mathcal{K} - \mathcal{P} + \mathcal{W})\,\mathrm{d}t = 0 \tag{9}$$

leads to the following partial differential equation:

$$\mu(z)\ddot{w} = -\,\partial^2_{z^2}\left(\kappa(z)\partial^2_{z^2} w\right) + \partial^2_{z^2}\left(\Pi_{ab}(z) k_p v(z,t)\right)\,, \tag{10}$$

where:

$$\begin{aligned}\mu(z) &:= \rho S + \rho_p S_p \Pi_{ab}(z)\,,\\ \kappa(z) &:= EI + \Pi_{ab}(z) E_p I_p\,,\\ k_p &:= \frac{\gamma I_{p,1}}{t_p}\,.\end{aligned} \tag{11}$$

2.2 Port-Hamiltonian representation

The system Hamiltonian is given by:

$$H[x_1, x_2] = \frac{1}{2}\int_{z=0}^{L}\left(\frac{x_1(z,t)^2}{\mu(z)} + \kappa(z) x_2(z,t)^2\right)\mathrm{d}z\,, \tag{12}$$

where $x_1(z,t)$ and $x_2(z,t)$ are the energy variables, defined as follows:

$$\begin{aligned} x_1(z,t) &:= \mu(z)\dot{w}(z,t)\\ x_2(z,t) &:= \partial^2_{z^2} w(z,t)\,.\end{aligned} \tag{13}$$

The variational derivatives of the Hamiltonian with respect to x_1 and x_2 are given by:

$$e_1(z,t) := \frac{\delta H}{\delta x_1} = \frac{x_1(z,t)}{\mu} = \dot{w}(z,t)$$
$$e_2(z,t) := \frac{\delta H}{\delta x_2} = \kappa(z)x_2(z,t) = (EI + \Pi_{ab}(z)E_pI_p)\,\partial_{z^2}^2 w\,. \tag{14}$$

The variables e_1 and e_2 are called co-energy variables. Notice that e_1 is the local vertical speed, and e_2 is the local bending moment.

Eq. 10 can thus be rewritten as:

$$\begin{bmatrix}\dot{x_1}\\ \dot{x_2}\end{bmatrix} = \underbrace{\begin{bmatrix}0 & -\partial_{z^2}^2\\ \partial_{z^2}^2 & 0\end{bmatrix}}_{\mathcal{J}}\begin{bmatrix}e_1\\ e_2\end{bmatrix} + \begin{bmatrix}\partial_{z^2}^2\\ 0\end{bmatrix}\Pi_{ab}(z)k_pv(z,t)\,, \tag{15}$$

where $\mathcal{J}$ is a formally skew-symmetric operator.

The time-derivative of the Hamiltonian is computed as:

$$\begin{aligned}\dot{H} &= \int_{z=0}^{L}(e_1\dot{x_1} + e_2\dot{x_2})\,\mathrm{d}z\,,\\ &= \int_{z=0}^{L}\left(e_1\left(-\partial_{z^2}^2e_2 + \partial_{z^2}^2\Pi_{ab}(z)k_pv(z,t)\right) + e_2\,\partial_{z^2}^2e_1\right)\mathrm{d}z\,,\\ &= \int_{z=0}^{L}\left(\partial_z\left(-e_1\,\partial_z(e_2) + \partial_z(e_1)\,e_2\right)\right.\\ &\qquad \left.+e_1\,\partial_{z^2}^2\Pi_{ab}(z)k_pv(z,t)\right)\mathrm{d}z\,,\\ &= \left(-e_1\,\partial_z(e_2) + \partial_z(e_1)e_2\right)\Big|_{z=0}^{L} + \int_{z=a}^{b}k_pv(z,t)\,\partial_{z^2}^2e_1\,\mathrm{d}z\,.\end{aligned} \tag{16}$$

The first part of $\dot{H}$ depends only on the boundary values of e_1 (vertical speed), e_2 (moment), $\partial_z e_1$ (rotation speed) and $\partial_z e_2$ (force). This motivates the definition of the boundary-ports, which allows writing the infinite-dimensional equations as port-Hamiltonian systems. From Eq. 16, one possible definition for the boundary ports is as follows [1]:

$$\boldsymbol{y}_\partial := \begin{bmatrix}f_{1\partial}\\ f_{2\partial}\\ f_{3\partial}\\ f_{4\partial}\end{bmatrix} := \begin{bmatrix}\partial_z\boldsymbol{e}_2(0)\\ -\boldsymbol{e}_2(0)\\ -\boldsymbol{e}_1(L)\\ \partial_z\boldsymbol{e}_1(L)\end{bmatrix},\ \boldsymbol{u}_\partial = \begin{bmatrix}e_{1\partial}\\ e_{2\partial}\\ e_{3\partial}\\ e_{4\partial}\end{bmatrix} = \begin{bmatrix}\boldsymbol{e}_1(0)\\ \partial_z\boldsymbol{e}_1(0)\\ \partial_z\boldsymbol{e}_2(L)\\ \boldsymbol{e}_2(L)\end{bmatrix}. \tag{17}$$

The second part of $\dot{H}$ depends on the distributed voltage $v(z,t)$. It also motivates us to define a power-conjugated output to $v(z,t)$ given by:

$$y(z,t) := k_p\,\partial_{z^2}^2e_1\,,\quad a < z < b\,. \tag{18}$$

The final energy flow ($\dot{H}$) can thus be written as:

$$\dot{H} = \boldsymbol{y}_\partial^T\boldsymbol{u}_\partial + \int_{z=a}^{b}v(z,t)y(z,t)\,\mathrm{d}z\,. \tag{19}$$

Remark 1. In practice, for a single piezoelectric patch $v(z,t) = v(t)$ (the voltage is uniform along the patch). In this case, $\dot{H}$ becomes:

$$\begin{aligned}\dot{H} &= \boldsymbol{y}_\partial^T\boldsymbol{u}_\partial + k_p\partial_ze_1\Big|_{z=a}^{b}v(t)\,,\\ &= \boldsymbol{y}_\partial^T\boldsymbol{u}_\partial + k_p\left(\partial_ze_1(b) - \partial_ze_1(a)\right)v(t)\end{aligned} \tag{20}$$

[1] Other choices are possible, see e.g. Le Gorrec et al. (2005)

The distributed case can be approximately implemented by using a set of small piezoelectric patches with different voltages applied.

Remark 2. In Eq. 15, the input operator is unbounded and the rectangular function is discontinuous. Despite of these difficulties, existence and uniqueness results for such systems can be found in (Banks et al., 1996, Chapter 4).

2.3 Weak formulation

Since in Eq. 15 the second-order derivative is applied to a nonsmooth rectangular function $\Pi_{ab}(z)$, we propose to use an integral formulation, with an arbitrary smooth test function $c(z)$:

$$\int_{z=0}^{L}c(z)\begin{bmatrix}\dot{x_1}\\ \dot{x_2}\end{bmatrix}\mathrm{d}z = \int_{z=0}^{L}c(z)\mathcal{J}\begin{bmatrix}e_1\\ e_2\end{bmatrix}\mathrm{d}z + \int_{z=0}^{L}c(z)\begin{bmatrix}\partial_{z^2}^2\\ 0\end{bmatrix}\Pi_{ab}(z)k_pv(z,t)\,\mathrm{d}z\,.$$

After integrating by parts twice, the weak formulation of the original problem is found to be:

$$\int_{z=0}^{L}c(z)\begin{bmatrix}\dot{x_1}\\ \dot{x_2}\end{bmatrix}\mathrm{d}z = \int_{z=0}^{L}c(z)\mathcal{J}\begin{bmatrix}e_1\\ e_2\end{bmatrix}\mathrm{d}z + \int_{z=a}^{b}\partial_{z^2}^2\left(c(z)\right)\begin{bmatrix}1\\ 0\end{bmatrix}k_pv(z,t)\,\mathrm{d}z\,. \tag{21}$$

Now, the second order derivative is applied to the smooth function $c(z)$. Moreover, thanks to clever choices for $c(z)$, the weak formulation will enable to set up efficient numerical methods, presented in Section 3.

3. POWER-PRESERVING DISCRETIZATION

This section is divided in four parts. Firstly, the approximation basis for each variable is presented. Secondly, the equations of motion presented in Eq. 21 are spatially discretized. Thirdly, the time-derivative of the Hamiltonian in the finite-dimension space is analyzed: this motivates the definition of new finite-dimensional co-energy and port-variables that guarantee the power-conservation of the system. Finally, the finite-dimensional equations together with the definition of the co-energy and port variables are combined in Section 3.4 to define a finite-dimensional port-Hamiltonian representation of the system.

3.1 Approximation basis

The idea of Moulla et al. (2012) is to approximate the energy and co-energy variables into a finite-dimensional space, using polynomial interpolation. Different degrees for the polynomial basis are used for each of these variables. Here, since $\mathcal{J}$ is a second-order operator, a degree N is chosen for the energy variables, and $N+2$ for the co-energy variables. Then, the operator $\mathcal{J}$ provides exact differential relations in the finite-dimensional spaces. For $j = 1, 2$:

$$x_j(z,t) \approx \sum_{i=1}^{N}x_j^i(t)\phi^i(z) = (\boldsymbol{x}_j)^T(t)\boldsymbol{\phi}(z)\,,\quad 0 < z < L\,, \tag{22}$$

$$e_j(z,t) \approx \sum_{i=1}^{N+2}e_j^i(t)\psi^i(z) = (\boldsymbol{e}_j)^T(t)\boldsymbol{\psi}(z)\,,\quad 0 < z < L\,, \tag{23}$$

An alternative approximation for the co-energy variables (this time of degree N) is defined using the same basis as the energy variables. This definition will be useful for approximating the distributed ports.

$$e_j(z,t) \approx \sum_{i=1}^{N} \hat{e}_j^i(t)\phi^i(z) = (\hat{\boldsymbol{e}}_j)^T(t)\boldsymbol{\phi}(z)\,, \quad 0 < z < L\,, \tag{24}$$

In addition, we approximate the distributed external input $v(z,t)$ using a degree K polynomial basis:

$$v(z,t) \approx \sum_{i=1}^{K} v^i(t)\theta^i(z) = \boldsymbol{v}^T(t)\boldsymbol{\theta}(z)\,, \quad a < z < b\,, \tag{25}$$

The same basis will be used to approximate the distributed output $y(z,t)$.

As done by Moulla et al. (2012)), we have used Lagrange polynomials as approximation basis. Other more problem-specific basis as Bessel functions can also be used (see e.g. Vu et al. (2013)). For Lagrange polynomials, the values of the coefficients $\boldsymbol{x_j}(t)$, $\boldsymbol{e_j}(t)$ and $\boldsymbol{v}(t)$ are the values of $x_j(z,t)$, $e_j(z,t)$ and $v(z,t)$ evaluated at the collocation points. The collocation points are denoted as z_{xi} for the energy space, z_{ei} for the co-energy space and z_{vi} for the distributed input. Note that the energy variables are approximated using N points, the co-energy variables using $N+2$ points, and the distributed external input using K collocation points.

3.2 Finite-dimensional equations

In Moulla et al. (2012), a collocation method was used, based directly on the strong formulation of the infinite-dimensional pHs. This method cannot be applied here because of the term $\partial_{z^2}^2\left(\Pi_{ab}(z)k_p v(z,t)\right)$ in the strong form of our problem (Eq. 15). In order to overcome this problem, the weak form of Section 2.3 is used, with the particular choice of $c(z) = \boldsymbol{c}^T\boldsymbol{\phi}(z)$, for an arbitrary vector $\boldsymbol{c}$. From the weak form Eq. 21, using the approximations from Eqs. 22, 23, 25, we get:

$$\begin{aligned}\left(\int_{z=0}^{L}\boldsymbol{\phi}\boldsymbol{\phi}^T\,\mathrm{d}z\right)\dot{\boldsymbol{x}}_1 &= -\left(\int_{z=0}^{L}\boldsymbol{\phi}\boldsymbol{\psi}_{zz}(z)^T\,\mathrm{d}z\right)\boldsymbol{e}_2 \\ &\quad + \left(\int_{z=a}^{b}\boldsymbol{\phi}_{zz}\boldsymbol{\theta}(z)^T\,\mathrm{d}z\right)k_p\boldsymbol{v}\,, \\ \left(\int_{z=0}^{L}\boldsymbol{\phi}\boldsymbol{\phi}^T\,\mathrm{d}z\right)\dot{\boldsymbol{x}}_2 &= \left(\int_{z=0}^{L}\boldsymbol{\phi}\boldsymbol{\psi}_{zz}(z)^T\,\mathrm{d}z\right)\boldsymbol{e}_1\,.\end{aligned} \tag{26}$$

In order to simplify the presentation, we define:

$$\begin{aligned}M_\phi &:= \int_{z=0}^{L}\boldsymbol{\phi}\boldsymbol{\phi}^T\,\mathrm{d}z\,, \\ \bar{D}_2 &:= \int_{z=0}^{L}\boldsymbol{\phi}\boldsymbol{\psi}_{zz}^T\,\mathrm{d}z\,, \\ \tilde{B} &:= k_p\int_{z=a}^{b}\boldsymbol{\phi}_{zz}\boldsymbol{\theta}^T\,\mathrm{d}z\,,\end{aligned} \tag{27}$$

M_ϕ is a symmetric positive-definite $N\times N$ matrix, $\bar{D}_2$ is an $N\times(N+2)$ matrix and $\tilde{B}$ is an $N\times K$ matrix.

The finite-dimensional equations (Eqs. 26) thus become:

$$\begin{aligned}M_\phi\dot{\boldsymbol{x}}_1 &= -\bar{D}_2\boldsymbol{e}_2 + \tilde{B}\boldsymbol{v} \\ M_\phi\dot{\boldsymbol{x}}_2 &= \bar{D}_2\boldsymbol{e}_1\end{aligned} \tag{28}$$

Definition 1. The differentiation matrix D_2 is defined as:

$$D_2 := \begin{bmatrix}\boldsymbol{\psi}_{zz}(z_{x1})^T \\ \boldsymbol{\psi}_{zz}(z_{x2})^T \\ \boldsymbol{\psi}_{zz}(z_{x3})^T \\ \vdots \\ \boldsymbol{\psi}_{zz}(z_{xN})^T\end{bmatrix} \tag{29}$$

where z_{xi} are the collocation points related to the energy variables approximation basis. D_2 is an $N\times(N+2)$ matrix.

Proposition 1. The differentiation matrix D_2 is equivalent to the matrix obtained from the weak formulation method, i.e.,

$$D_2 = M_\phi^{-1}\bar{D}_2\,. \tag{30}$$

Proof. Let $f(z) := \boldsymbol{f}^T\boldsymbol{\phi}(z)$ be a polynomial of degree N, $g(z) := \boldsymbol{g}^T\boldsymbol{\psi}(z)$ a polynomial of degree $N+2$. If $f(z) = \partial_{z^2}^2 g(z)$:

$$\boldsymbol{f}^T\boldsymbol{\phi}(z) = \boldsymbol{g}^T\boldsymbol{\psi}_{zz}(z)\,,$$

evaluating the previous expression at each collocation point z_{xi}:

$$\begin{aligned}\boldsymbol{f} &= D_2\boldsymbol{g}\,, \\ \boldsymbol{g}^T D_2^T\boldsymbol{\phi}(z) &= \boldsymbol{g}^T\boldsymbol{\psi}_{zz}(z)\,.\end{aligned} \tag{31}$$

Since both $\boldsymbol{f}^T\boldsymbol{\phi}(z)$ and $\boldsymbol{g}^T\boldsymbol{\psi}_{zz}(z)$ are polynomials of degree N, the previous equation is exact for any $\boldsymbol{g}$ and:

$$\boldsymbol{\phi}^T D_2 = \boldsymbol{\psi}_{zz}^T\,. \tag{32}$$

We can multiply it by $\boldsymbol{\phi}$ and integrate over $(0,L)$:

$$\int_{z=0}^{L}\boldsymbol{\phi}\boldsymbol{\phi}^T\,\mathrm{d}z\,D_2 = \int_{z=0}^{L}\boldsymbol{\phi}\boldsymbol{\psi}_{zz}^T\,\mathrm{d}z\,. \tag{33}$$

$$M_\phi D_2 = \bar{D}_2\,. \tag{34}$$

Finally:

$$D_2 = M_\phi^{-1}\bar{D}_2\,. \tag{35}$$

□

Multiplying Eqs. 28 by M_ϕ^{-1} and using Proposition 1, we find the final finite-dimensional equations:

$$\begin{aligned}\dot{\boldsymbol{x}}_1 &= -D_2\boldsymbol{e}_2 + M_\phi^{-1}\tilde{B}\boldsymbol{v}\,, \\ \dot{\boldsymbol{x}}_2 &= D_2\boldsymbol{e}_1\,.\end{aligned} \tag{36}$$

3.3 Time-derivative of the Hamiltonian and port variables

In this section, we will analyze the time-derivative of the Hamiltonian in the finite-dimensional space. This analysis will motivate the definition of new co-energy and port-variables, that, together with Eq. 36, will allow us to write the approximated system in the classical finite-dimensional port-Hamiltonian framework in Section 3.4.

From the definition of the variational derivative:

$$\begin{aligned}\dot{H} &= \int_{z=0}^{L}\left(\delta_{x_1}H\,\dot{x}_1 + \delta_{x_2}H\,\dot{x}_2\right)\mathrm{d}z\,, \\ &= \int_{z=0}^{L}\left(e_1\dot{x}_1 + e_2\dot{x}_2\right)\mathrm{d}z\,,\end{aligned} \tag{37}$$

after substitution of the approximated $x_j(z,t)$ and $e_j(z,t)$, we get:

$$\dot{H} \approx \boldsymbol{e}_1^T M_{\psi\phi}\dot{\boldsymbol{x}}_1 + \boldsymbol{e}_2^T M_{\psi\phi}\dot{\boldsymbol{x}}_2\,, \tag{38}$$

where:

$$M_{\psi\phi} := \int_{z=0}^{L} \boldsymbol{\psi}(z)\boldsymbol{\phi}^T(z)\,\mathrm{d}z \tag{39}$$

is an $(N+2)\times N$ matrix.

Definition 2. The discretized Hamiltonian H_d is defined as:

$$H_d(\boldsymbol{x}_1,\boldsymbol{x}_2) := H[x_1(x,t)=\boldsymbol{x}_1^T\boldsymbol{\phi}(z), x_2(x,t)=\boldsymbol{x}_2^T\boldsymbol{\phi}(z)]\,.$$

The time-derivative of the H_d is given by:

$$\dot{H}_d(\boldsymbol{x}_1,\boldsymbol{x}_1) = \frac{\partial H_d}{\partial \boldsymbol{x}_1}^T \dot{\boldsymbol{x}}_1 + \frac{\partial H_d}{\partial \boldsymbol{x}_1}^T \dot{\boldsymbol{x}}_1\,, \tag{40}$$

where $\frac{\partial H_d}{\partial \boldsymbol{x}_i}$ is the gradient of H_d with respect to $\boldsymbol{x}_i$ (it is a vector of dimension N). We want that both approximations (Eqs. 38 and 40) coincide: this motivates us to define new co-energy variables $\tilde{\boldsymbol{e}}_i$:

$$\begin{aligned}\tilde{\boldsymbol{e}}_1 = M_{\psi\phi}^T\boldsymbol{e}_1 = \frac{\partial H_d}{\partial \boldsymbol{x}_1}\,,\\ \tilde{\boldsymbol{e}}_2 = M_{\psi\phi}^T\boldsymbol{e}_2 = \frac{\partial H_d}{\partial \boldsymbol{x}_2}\,.\end{aligned} \tag{41}$$

Proposition 2. This newly defined $N-$dimensional co-energy variable $\tilde{\boldsymbol{e}}_j$ can be related to the previously defined $N-$dimensional pointwise co-energy variable approximation $\hat{\boldsymbol{e}}_j$ as:

$$\hat{\boldsymbol{e}}_j = M_\phi^{-1}\tilde{\boldsymbol{e}}_j\,,\quad j=1,2\,, \tag{42}$$

such that both approximations will equally approximate the system energy flow.

Proof. When using $e_j(z,t)\approx\hat{\boldsymbol{e}}_j^T\boldsymbol{\phi}$, the energy flow becomes:

$$\begin{aligned}\dot{H} &= \hat{\boldsymbol{e}}_1^T\left(\int_{z=0}^{L}\boldsymbol{\phi}\boldsymbol{\phi}^T\,\mathrm{d}z\right)\dot{\boldsymbol{x}}_1 + \hat{\boldsymbol{e}}_2^T\left(\int_{z=0}^{L}\boldsymbol{\phi}\boldsymbol{\phi}^T\,\mathrm{d}z\right)\dot{\boldsymbol{x}}_2\,,\\ &= \hat{\boldsymbol{e}}_1^T M_\phi\dot{\boldsymbol{x}}_1 + \hat{\boldsymbol{e}}_2^T M_\phi\dot{\boldsymbol{x}}_2\end{aligned}$$

But from Eq. 38 and 41:

$$\dot{H} = \tilde{\boldsymbol{e}}_1^T\dot{\boldsymbol{x}}_1 + \tilde{\boldsymbol{e}}_2^T\dot{\boldsymbol{x}}_2\,,$$

so to satisfy both energy flows, the following equality must hold:

$$\hat{\boldsymbol{e}}_j = M_\phi^{-1}\tilde{\boldsymbol{e}}_j\,.$$

□

After substitution of the finite-dimensional equations (Eqs. 36) in Eq. 40:

$$\begin{aligned}\dot{H}_d &= -\tilde{\boldsymbol{e}}_1^T\left(D_2\boldsymbol{e}_2 + M_\phi^{-1}\tilde{B}\boldsymbol{v}\right) + \tilde{\boldsymbol{e}}_2^T D_2\boldsymbol{e}_1\,,\\ &= -\boldsymbol{e}_1^T\left(M_{\psi\phi}D_2\boldsymbol{e}_2 + M_{\psi\phi}M_\phi^{-1}\tilde{B}\boldsymbol{v}\right) + \boldsymbol{e}_2^T M_{\psi\phi}D_2\boldsymbol{e}_1\,,\\ &= \boldsymbol{e}_1^T\left(-M_{\psi\phi}D_2 + D_2^T M_{\psi\phi}^T\right)\boldsymbol{e}_2 + \boldsymbol{e}_1^T M_{\psi\phi}M_\phi^{-1}\tilde{B}\boldsymbol{v}\,.\end{aligned} \tag{43}$$

Proposition 3. As it happened in the infinite-dimensional case (Eq. 16), the first part of the energy flow in Eq. 43 is related to the boundary conditions, so that:

$$\begin{aligned}\boldsymbol{e}_1^T\left(-M_{\psi\phi}D_2 + D_2^T M_{\psi\phi}^T\right)\boldsymbol{e}_2 = &-\boldsymbol{e}_1^T\boldsymbol{\psi}(z)\boldsymbol{\psi}_z^T(z)\boldsymbol{e}_2\Big|_{z=0}^{L}\\ &+\boldsymbol{e}_1^T\boldsymbol{\psi}_z(z)\boldsymbol{\psi}^T(z)\boldsymbol{e}_2\Big|_{z=0}^{L}\,.\end{aligned} \tag{44}$$

Proof.

$$\begin{aligned}&\boldsymbol{e}_1^T\left(-M_{\psi\phi}D_2 + D_2^T M_{\psi\phi}^T\right)\boldsymbol{e}_2\\ &= \boldsymbol{e}_1^T\left(-\int_{z=0}^{L}\boldsymbol{\psi}(z)\boldsymbol{\phi}^T(z)\,\mathrm{d}z D_2 + D_2^T\int_{z=0}^{L}\boldsymbol{\phi}(z)\boldsymbol{\psi}^T(z)\,\mathrm{d}z\right)\boldsymbol{e}_2\,,\\ &= \boldsymbol{e}_1^T\left(-\int_{z=0}^{L}\boldsymbol{\psi}(z)\boldsymbol{\phi}^T(z)D_2\,\mathrm{d}z + \int_{z=0}^{L}D_2^T\boldsymbol{\phi}(z)\boldsymbol{\psi}^T(z)\,\mathrm{d}z\right)\boldsymbol{e}_2\,.\end{aligned} \tag{45}$$

Since $\boldsymbol{\phi}^T D_2 = \boldsymbol{\psi}_{zz}^T$ (Eq. 32):

$$\begin{aligned}&\boldsymbol{e}_1^T\left(-M_{\psi\phi}D_2 + D_2^T M_{\psi\phi}^T\right)\boldsymbol{e}_2\\ &= \boldsymbol{e}_1^T\left(-\int_{z=0}^{L}\boldsymbol{\psi}(z)\boldsymbol{\psi}_{zz}\,\mathrm{d}z + \int_{z=0}^{L}\boldsymbol{\psi}_{zz}\boldsymbol{\psi}^T(z)\,\mathrm{d}z\right)\boldsymbol{e}_2\,,\\ &= \boldsymbol{e}_1^T\left(\int_{z=0}^{L}\partial_z\left(-\boldsymbol{\psi}(z)\boldsymbol{\psi}_z^T(z) + \boldsymbol{\psi}_z(z)\boldsymbol{\psi}^T(z)\right)\mathrm{d}z\right)\boldsymbol{e}_2\,,\\ &= \boldsymbol{e}_1^T\left(-\boldsymbol{\psi}(z)\boldsymbol{\psi}_z^T(z) + \boldsymbol{\psi}_z(z)\boldsymbol{\psi}^T(z)\right)\boldsymbol{e}_2\Big|_{z=0}^{L}\,.\end{aligned} \tag{46}$$

□

From the above equations, one possible definition for the boundary ports is as follows:

$$\boldsymbol{y}_\partial := \begin{bmatrix}f_{1\partial}\\ f_{2\partial}\\ f_{3\partial}\\ f_{4\partial}\end{bmatrix} := \begin{bmatrix}\boldsymbol{\psi}_z^T(0)\boldsymbol{e}_2\\ -\boldsymbol{\psi}^T(0)\boldsymbol{e}_2\\ -\boldsymbol{\psi}^T(L)\boldsymbol{e}_1\\ \boldsymbol{\psi}_z^T(L)\boldsymbol{e}_1\end{bmatrix},\ \boldsymbol{u}_\partial = \begin{bmatrix}e_{1\partial}\\ e_{2\partial}\\ e_{3\partial}\\ e_{4\partial}\end{bmatrix} = \begin{bmatrix}\boldsymbol{\psi}^T(0)\boldsymbol{e}_1\\ \boldsymbol{\psi}_z^T(0)\boldsymbol{e}_1\\ \boldsymbol{\psi}_z^T(L)\boldsymbol{e}_2\\ \boldsymbol{\psi}^T(L)\boldsymbol{e}_2\end{bmatrix}. \tag{47}$$

The approximated Hamiltonian time derivative is thus written as:

$$\dot{H}_d = \boldsymbol{y}_\partial^T\boldsymbol{u}_\partial + \tilde{\boldsymbol{e}}_1^T M_\phi^{-1}\tilde{B}\boldsymbol{v}\,. \tag{48}$$

The second part of the energy flow is related to the distributed ports. The previous expression readily motivates us to define the output conjugated to $\boldsymbol{v}$:

$$\boldsymbol{v}^* = \tilde{B}^T M_\phi^{-1}\tilde{\boldsymbol{e}}_1 \tag{49}$$

Proposition 4. The previous conjugated output can be obtained from the spatial discretization of the infinite-dimensional output: $y(z,t) = k_p\partial_{z^2}^2 e_1(z,t)$. In addition, this finite-dimensional conjugated output preserves the original energy flow related to the distributed ports $\int_{z=a}^{b} y(z,t)v(z,t)\,\mathrm{d}z$ in the finite-dimensional space.

Proof. Let us approximate $e_1(z,t)$ using the $N-$dimensional basis:

$$e_1(z,t)\approx\hat{\boldsymbol{e}}_1^T(t)\boldsymbol{\phi}(z)\,,$$

and $y(z,t)$ by:

$$y(z,t)\approx\boldsymbol{y}^T(t)\boldsymbol{\theta}(z)\,.$$

The approximated equations become:

$$\boldsymbol{\theta}^T\boldsymbol{y} = k_p\boldsymbol{\phi}_{zz}^T\hat{\boldsymbol{e}}_1\,.$$

Multiplying by $\boldsymbol{\theta}$ and integrating over (a,b):

$$\left(\int_{z=a}^{b}\boldsymbol{\theta}\boldsymbol{\theta}^T\,\mathrm{d}z\right)\boldsymbol{y} = k_p\left(\int_{z=a}^{b}\boldsymbol{\theta}\boldsymbol{\phi}_{zz}^T\,\mathrm{d}z\right)\hat{\boldsymbol{e}}_1\,,$$

Since $\hat{\boldsymbol{e}}_1 = M_\phi^{-1}\tilde{\boldsymbol{e}}_1$, we find $\boldsymbol{v}^*$:

$$\boldsymbol{v}^* = M_\theta\,\boldsymbol{y} = \tilde{B}M_\phi^{-1}\tilde{\boldsymbol{e}}_1\,,$$

where $M_\theta := \int_{z=a}^{b}\boldsymbol{\theta}\boldsymbol{\theta}^T\,\mathrm{d}z$ is a symmetric positive-definite $K\times K$ matrix.

Looking at the energy flow discretization:

$$\begin{aligned}\int_{z=a}^{b} y(z,t)v(z,t)\,\mathrm{d}z \approx \int_{z=a}^{b} \boldsymbol{y}^T\boldsymbol{\theta}\boldsymbol{\theta}^T\boldsymbol{v}\,\mathrm{d}z\,,\\ =\boldsymbol{y}^T M_\theta\,\boldsymbol{v}\,,\\ =(\boldsymbol{v}^*)^T\boldsymbol{v}\,.\end{aligned}$$

□

From Eq. 48 and the previous proposition, we have the final energy flow of the finite-dimensional system:

$$\dot{H}_d = \boldsymbol{y}_\partial^T\boldsymbol{u}_\partial + (\boldsymbol{v}^*)^T\boldsymbol{v}\,. \tag{50}$$

3.4 Finite-dimensional port-Hamiltonian representation

We define the flow variables

$$\boldsymbol{f}^T := \left[-\dot{\boldsymbol{x}}_1\ f_{1\partial}\ f_{2\partial}\ -\dot{\boldsymbol{x}}_2\ f_{3\partial}\ f_{4\partial}\ \boldsymbol{v}^*\right]^T\,, \tag{51}$$

and the effort variables as

$$\boldsymbol{e}^T := \left[\tilde{\boldsymbol{e}}_1\ e_{1\partial}\ e_{2\partial}\ \tilde{\boldsymbol{e}}_2\ e_{3\partial}\ e_{4\partial}\ \boldsymbol{v}\right]^T\,, \tag{52}$$

where both $\boldsymbol{f}$ and $\boldsymbol{e} \in R^{2N+4+K}$.

Using the finite-dimensional Eqs. 36, the co-energy variables definition from Eq. 41, the boundary-ports definition from Eq. 47 and the distributed ports definition from Eq. 49, it is possible to write:

$$\begin{bmatrix}-\dot{\boldsymbol{x}}_1\\ f_{1\partial}\\ f_{2\partial}\\ -\dot{\boldsymbol{x}}_2\\ f_{3\partial}\\ f_{4\partial}\\ \boldsymbol{v}^*\end{bmatrix} = \begin{bmatrix}0 & D_2 & -M_\phi^{-1}\tilde{B}\\ 0 & \boldsymbol{\psi}_z^T(0) & 0\\ 0 & -\boldsymbol{\psi}^T(0) & 0\\ -D_2 & 0 & 0\\ -\boldsymbol{\psi}^T(L) & 0 & 0\\ \boldsymbol{\psi}_z^T(L) & 0 & 0\\ \tilde{B}^T M_\phi^{-1} M_{\psi\phi}^T & 0 & 0\end{bmatrix}\begin{bmatrix}\boldsymbol{e}_1\\ \boldsymbol{e}_2\\ \boldsymbol{v}\end{bmatrix}, \tag{53}$$

$$\begin{bmatrix}\tilde{\boldsymbol{e}}_1\\ e_{1\partial}\\ e_{2\partial}\\ \tilde{\boldsymbol{e}}_2\\ e_{3\partial}\\ e_{4\partial}\\ \boldsymbol{v}\end{bmatrix} = \begin{bmatrix}M_{\psi\phi}^T & 0 & 0\\ \boldsymbol{\psi}^T(0) & 0 & 0\\ \boldsymbol{\psi}_z^T(0) & 0 & 0\\ 0 & M_{\psi\phi}^T & 0\\ 0 & \boldsymbol{\psi}_z^T(L) & 0\\ 0 & \boldsymbol{\psi}^T(L) & 0\\ 0 & 0 & I\end{bmatrix}\begin{bmatrix}\boldsymbol{e}_1\\ \boldsymbol{e}_2\\ \boldsymbol{v}\end{bmatrix}. \tag{54}$$

Together with the Hamiltonian H_d and its gradient ($\tilde{\boldsymbol{e}}_1$ and $\tilde{\boldsymbol{e}}_2$), Eqs. 53 and 54 provide an image representation of port-Hamiltonian system (see e.g. Duindam et al. (2009)). These equations can be rewritten in explicit form as [2]:

$$\begin{bmatrix}-\dot{\boldsymbol{x}}_1\\ f_{1\partial}\\ f_{2\partial}\\ -\dot{\boldsymbol{x}}_2\\ f_{3\partial}\\ f_{4\partial}\\ \boldsymbol{v}^*\end{bmatrix} = \tilde{J}\begin{bmatrix}\tilde{\boldsymbol{e}}_1\\ e_{1\partial}\\ e_{2\partial}\\ \tilde{\boldsymbol{e}}_2\\ e_{3\partial}\\ e_{4\partial}\\ \boldsymbol{v}\end{bmatrix}, \tag{55}$$

where:

$$\tilde{J} = \begin{bmatrix}0 & \begin{pmatrix}D_2\\ \boldsymbol{\psi}_z^T(0)\\ -\boldsymbol{\psi}^T(0)\end{pmatrix}\begin{pmatrix}M_{\psi\phi}^T\\ \boldsymbol{\psi}_z^T(L)\\ \boldsymbol{\psi}^T(L)\end{pmatrix}^{-1} & -M_\phi^{-1}\tilde{B}\\ \begin{pmatrix}-D_2\\ -\boldsymbol{\psi}^T(L)\\ \boldsymbol{\psi}_z^T(L)\end{pmatrix}\begin{pmatrix}M_{\psi\phi}^T\\ \boldsymbol{\psi}^T(0)\\ \boldsymbol{\psi}_z^T(0)\end{pmatrix}^{-1} & 0 & 0\\ \tilde{B}^T M_\phi^{-1} & 0 & 0\end{bmatrix} \tag{56}$$

Skew-symmetry of $\tilde{J}$ is easily proved by the scalar product between flow and effort variables (Eqs. 53 and 54), which is equal to:

$$\begin{aligned}\boldsymbol{e}_1^T\big(M_{\psi\phi}D_2 - D_2^T M_{\psi\phi}^T - \boldsymbol{\psi}(L)\boldsymbol{\psi}_z^T(L) + \boldsymbol{\psi}_z(L)\boldsymbol{\psi}^T(L)\\ -\boldsymbol{\psi}(0)\boldsymbol{\psi}_z^T(0) + \boldsymbol{\psi}_z(0)\boldsymbol{\psi}^T(0)\big)\,\boldsymbol{e}_2,\end{aligned} \tag{57}$$

But from Proposition 3, the previous expression is equal to zero. So, Eq. 55 is a finite-dimensional approximation of Eq. 15 that preserves the skew-symmetry property of the original infinite-dimensional system at the discrete level.

Finally, it is possible to rewrite Eq. 55 in a more classical way, by simply rearranging its rows and columns:

$$\begin{bmatrix}-\dot{\boldsymbol{x}}\\ \boldsymbol{y}_\partial\\ \boldsymbol{y}_d\end{bmatrix} = \begin{bmatrix}-J & -B_\partial & -B_d\\ B_\partial^T & D_\partial & 0\\ B_d^T & 0 & 0\end{bmatrix}\begin{bmatrix}\tilde{\boldsymbol{e}}\\ \boldsymbol{u}_\partial\\ \boldsymbol{u}_d\end{bmatrix}, \tag{58}$$

where $\dot{\boldsymbol{x}} = \left[\dot{\boldsymbol{x}}_1^T\ \dot{\boldsymbol{x}}_2^T\right]^T$, $\tilde{\boldsymbol{e}} = \left[\tilde{\boldsymbol{e}}_1\ \tilde{\boldsymbol{e}}_2\right]^T$, $\boldsymbol{u}_\partial$ and $\boldsymbol{y}_\partial$ are the boundary inputs and outputs, $\boldsymbol{u}_d = \boldsymbol{v}$ and $\boldsymbol{y}_d = \boldsymbol{v}^*$ are the discretized distributed input/outputs. In addition, remember that $\tilde{\boldsymbol{e}}_j = \frac{\partial H_d}{\partial \boldsymbol{x}_j}$. J and D_∂ are skew-symmetric matrices.

The passivity property is also preserved, since $\dot{H}_d = \boldsymbol{y}_\partial^T\boldsymbol{u}_\partial + \boldsymbol{y}_d^T\boldsymbol{u}_d$.

4. NUMERICAL RESULTS AND EXPERIMENTAL VALIDATION

Since polynomial basis were used in this paper, the numerical computation of the matrices D_2, M_ϕ, $M_{\psi\phi}$ and $\tilde{B}$ can be easily handled through symbolic algebra software: this leads to exact computation of these matrices, but computational burden becomes too high even for not so large values of N (about 10). Another choice is to compute the integrals by exact quadrature formulas. The derivatives can be exactly computed using automatic differentiation algorithms [3] (allowing N of the order of hundreds with very small computational cost).

Gauss-Legendre collocation points were used. This choice reduces the high frequency oscillations, known as the Runge's phenomenon, since these points are more densely distributed near the edges of the interval (see e.g. Trefethen (2000)). In addition, when using these points, the matrix M_ϕ becomes diagonal (so it can be trivially inverted).

The active flexible structure of ISAE was used to validate the proposed numerical method. In this paper, the experimental device consists of a free-clamped plate controlled by two piezoelectric patches attached near the fixed end, as presented in Figs. 2 and 3. The tank is not taken into account. The plate characteristics are presented in Table 1

[2] The matrices $\begin{pmatrix}M^T\\ \boldsymbol{\psi}_z^T(0)\\ \boldsymbol{\psi}^T(0)\end{pmatrix}$ and $\begin{pmatrix}M_{\psi\phi}^T\\ \boldsymbol{\psi}^T(L)\\ \boldsymbol{\psi}_z^T(L)\end{pmatrix}$ are square and supposed to be invertible.

[3] We used the ForwardDiff package: http://www.juliadiff.org

and the piezoelectric patches characteristics are presented in Table 2. The movement of the plate is measured using an accelerometer located near the plate free-tip.

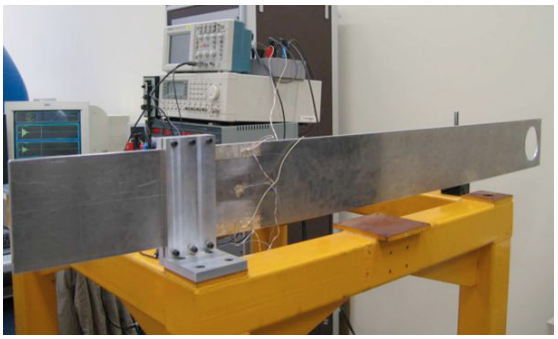

Fig. 2. Photo of the flexible plate.

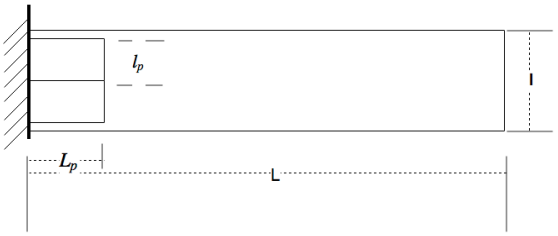

Fig. 3. Plate and piezoelectric patches schematic representation.

Table 1. Aluminum plate data.

Length	L	1.36 m
Width	l	0.16 m
Thickness	t	0.005 m
Density	ρ	2970 kg m^{-3}
Young modulus	E	75 GPa

Table 2. Piezoelectric patches data.

Length	L_p	0.14 m
Width	l_p	0.075 m
Thickness	t_p	0.0005 m
Density	ρ_p	7800 kg m^{-3}
Young modulus	E_p	67 GPa
Piezoelectric coefficient	d_{31}	$-2.1 \times 10^{-10} mV^{-1}$

The Euler-Bernoulli equation with constant coefficients and clamped-free boundary conditions have a well-known closed-form solution (obtained by using the method of separation of variables and modal decomposition), which we call the "exact" solution. This result was used to verify the accuracy of the numerical method.

Table 3 gives the natural frequencies obtained using the numerical method and compared to the "exact" results. Even with a small number of discretization points ($N = 12$), the first natural frequencies have errors limited by the numerical accuracy of the double-precision floating points (almost 15 significant decimal digits). The first 7 natural frequencies have less than 1% error.

Fig. 4 shows the frequency response of the system (voltage as input and speed at the free-tip as output). The figure shows an excellent agreement between the numerically-obtained system and the closed-form one. However, the experimental curve is shifted both in frequency and amplitude. The reason is that we neglected the piezoelectric patch rigidity and mass (to compare with the exact solutions).

Table 3. Natural frequencies obtained from the discretization method for the uniform beam.

6 elements		9 elements		12 elements		Exact
Freq.	Error	Freq.	Error	Freq.	Error	Freq.
2.19	2e-10	2.19	2e-14	2.19	4e-15	2.19
13.75	3e-05	13.75	1e-11	13.75	2e-14	13.75
38.53	6e-04	38.51	2e-06	38.51	2e-12	38.51
82.62	9e-02	75.46	3e-05	75.46	1e-07	75.46
146.74	2e-01	125.92	9e-03	124.74	2e-06	124.74
3446.40	2e+01	190.54	2e-02	186.51	9e-04	186.34
NaN	NaN	364.47	4e-01	261.00	3e-03	260.26

Finally, Fig. 5 shows the frequency response obtained from the numerical method, but with the piezoelectric patch rigidity and mass taken into account. The figure shows a good agreement between the numerical and experimental results.

The larger peaks of the numerical frequency response are due to the fact that damping was neglected in the modeling. This should be included in further work (see e.g. Matignon and Hélie (2013)).

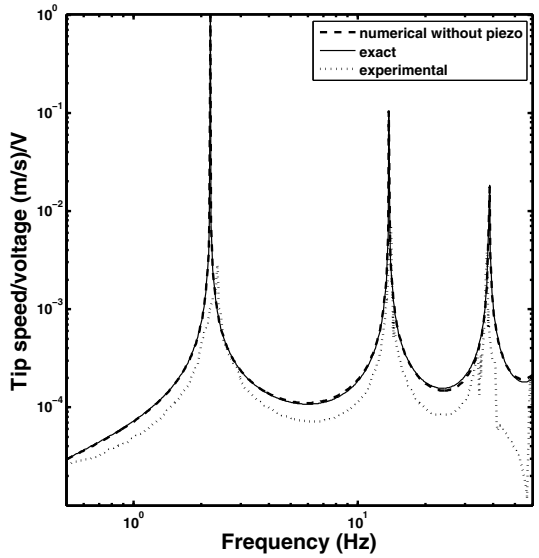

Fig. 4. Frequency response: numerical results using constant parameters (no piezoelectric patch rigidity and mass are taken into account).

5. CONCLUSION AND FURTHER WORK

The main goal of this paper was to find a finite-dimensional piezoelectric model that preserves the port-Hamiltonian structure of the infinite-dimensional system, which will be used for modeling and control of fluid-structure coupled systems. The final equations (Eq. 58) is a classical finite-dimensional port-Hamiltonian system, where the inputs/outputs are the boundary and distributed ports. The model was validated by comparisons with experimental results.

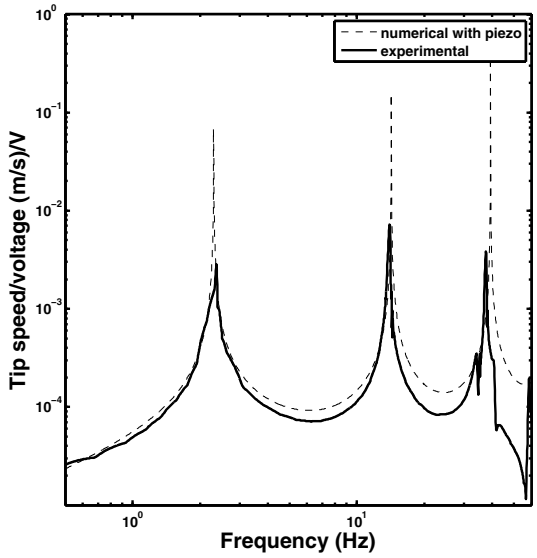

Fig. 5. Frequency response: numerical results taking the piezoelectric rigidity and mass into account.

Differently from previous work of structure-preserving discretization of piezoelectric beams, which used mixed-finite elements (based on the work of Golo et al. (2004)), this work uses global approximating functions (based on the work of Moulla et al. (2012)). This leads to an accurate (and small-order) finite-dimensional approximation. The numerical method was modified since the equations have an unbounded input operator (a second-order derivative of a rectangular function). For this reason, we use a weak-formulation instead of the strong-form equations.

In this work, the fixed-free conditions were used for the boundary ports (which means $\boldsymbol{u}_\partial = 0$). In further work, the free-tip boundary ports will be used to couple with the fluid dynamics in a consistent way. In addition, we are working in the design of control laws that take advantage of the port-Hamiltonian structure of the system.

The beam model used here is very simple, which is enough for simulating low-frequency phenomena of long beams (which is the case of our experimental device). To get a more accurate model, the method should be extended using for e.g. nonlinear Euler-Bernoulli and Timoshenko equations.

Finally, distributed ports were used here as control input. An additional interest of the distributed ports discretization method proposed here that should be explored in further work is to use them as interconnection ports. This can be used to couple different port-Hamiltonian systems using distributed ports instead of boundary-ports, guaranteeing that the energy is conserved.

REFERENCES

Aglietti, G.S., Gabriel, S.B., Langley, R.S., and Rogers, E. (1997). A modeling technique for active control design studies with application to spacecraft microvibrations. *The Journal of the Acoustical Society of America*, 102(4), 2158–66.

Banks, H.T., Smith, R.C., and Wang, Y. (1996). *Smart material structures: modeling, estimation, and control*. Wiley.

Boyd, J.P. (2001). *Chebyshev and Fourier Spectral Methods: Second Revised Edition*. Dover.

Cardoso-Ribeiro, F.L., Matignon, D., and Pommier-Budinger, V. (2015). Modeling of a Fluid-structure coupled system using port-Hamiltonian formulation. In *5th IFAC Workshop on Lagrangian and Hamiltonian Methods for Nonlinear Control LHMNC*, volume 48, 217–222. Lyon, France.

Duindam, V., Macchelli, A., and Stramigioli, S. (2009). *Modeling and Control of Complex Physical Systems*. Springer.

Geradin, M. and Rixen, D.J. (2015). *Mechanical Vibrations: Theory and Application to Structural Dynamics*. John Wiley & Sons.

Golo, G., Talasila, V., van der Schaft, A., and Maschke, B. (2004). Hamiltonian discretization of boundary control systems. *Automatica*, 40(5), 757–771.

Le Gorrec, Y., Zwart, H., and Maschke, B. (2005). Dirac structures and boundary control systems associated with skew-symmetric differential operators. *SIAM journal on control and optimization*, 44(5), 1864–1892.

Macchelli, A., van der Schaft, A., and Melchiorri, C. (2004). Multi-variable port Hamiltonian model of piezoelectric material. In *IEEE/RSJ International Conference on Intelligent Robots and Systems (IROS)*, volume 1. Sendai, Japan.

Matignon, D. and Hélie, T. (2013). A class of damping models preserving eigenspaces for linear conservative port-Hamiltonian systems. *European Journal of Control*, 19(6), 486–494.

Morris, K. and Ozer, A.O. (2013). Strong stabilization of piezoelectric beams with magnetic effects. In *52nd IEEE Conference on Decision and Control*, 3014–3019. Florence, Italy.

Moulla, R., Lefevre, L., and Maschke, B. (2012). Pseudo-spectral methods for the spatial symplectic reduction of open systems of conservation laws. *Journal of Computational Physics*, 231(4), 1272–1292.

Preumont, A. (2011). *Vibration Control of Active Structures*, volume 179. Springer.

Trefethen, L.N. (2000). *Spectral Methods in MATLAB*. Society for Industrial and Applied Mathematics.

Voss, T. and Scherpen, J. (2011). Structure preserving spatial discretization of a 1-D piezoelectric Timoshenko beam. *Multiscale Modeling & Simulation*, 9(1), 129–154.

Voss, T. and Scherpen, J. (2014). Port-Hamiltonian Modeling of a Nonlinear Timoshenko Beam with Piezo Actuation. *SIAM Journal on Control and Optimization*, 52(1), 493–519.

Voss, T. (2010). *Port-Hamiltonian Modeling and Control of Piezoelectric Beams and Plates: Application to Inflatable Space Structures*. Ph.D. thesis, University of Groningen.

Vu, N., Lefevre, L., Nouailletas, R., and Bremond, S. (2013). Geometric Discretization for a Plasma Control Model. In *5th IFAC Symposium on System Structure and Control*, 755–760. Grenoble, France.